Draft version July 20, 2016
Preprint typeset using LaTeX style emulateapj v. 08/22/09



# Q1549-C25: A CLEAN SOURCE OF LYMAN-CONTINUUM EMISSION AT $Z = 3.15$[1]

Alice E. Shapley,[2] Charles C. Steidel,[3] Allison L. Strom,[3] Milan Bogosavljević,[4] Naveen A. Reddy,[5] Brian Siana,[5] Robin E. Mostardi,[6] Gwen C. Rudie[7]

*Draft version July 20, 2016*

## ABSTRACT

We present observations of Q1549-C25, an $\sim L^*$ star-forming galaxy at $z = 3.15$ for which Lyman-continuum (LyC) radiation is significantly detected in deep Keck/LRIS spectroscopy. We find no evidence for contamination from a lower-redshift interloper close to the line of sight in the high signal-to-noise spectrum of Q1549-C25. Furthermore, the morphology of Q1549-C25 in $V_{606}$, $J_{125}$, and $H_{160}$ *Hubble Space Telescope* (*HST*) imaging reveals that the object consists of a single, isolated component within 1". In combination, these data indicate Q1549-C25 as a *clean* spectroscopic detection of LyC radiation, only the second such object discovered to date at $z \sim 3$. We model the spectral energy distribution (SED) of Q1549-C25, finding evidence for negligible dust extinction, an age (assuming continuous star formation) of $\sim 1$ Gyr, and a stellar mass of $M_* = 7.9 \times 10^9 M_\odot$. Although it is not possible to derive strong constraints on the absolute escape fraction of LyC emission, $f_{\rm esc}$(LyC), from a single object, we use simulations of intergalactic and circumgalactic absorption to infer $f_{\rm esc}$(LyC) $\geq$ 0.51 at 95% confidence. The combination of deep Keck/LRIS spectroscopy and *HST* imaging is required to assemble a larger sample of objects like Q1549-C25, and obtain robust constraints on the average $f_{\rm esc}$(LyC) at $z \sim 3$ and beyond.

*Subject headings:* cosmology: observations — diffuse radiation — galaxies: high-redshift — intergalactic medium

## 1. INTRODUCTION

The escape fraction of Lyman-continuum (LyC) photons from galaxies is a crucial component of models of the reionization of the universe. In recent reionization models, many reasonable assumptions have been adopted or constraints derived for the LyC escape fraction ($f_{\rm esc}$(LyC)) (e.g., Robertson et al. 2015; Finkelstein et al. 2012). However, such constraints are typically indirect (Kuhlen & Faucher-Giguère 2012) and do not substitute for the actual detection of ionizing photons leaking from galaxies. Because of the increasing intergalactic medium (IGM) optical depth at higher redshifts, it is not possible to directly measure escaping ionizing radiation from galaxies much beyond $z \sim 3$, let alone during the epoch of reionization (Vanzella et al. 2012). Therefore, such measurements must be performed at $z \leq 3.5$, the highest redshift at which IGM absorption does not destroy the signal of interest.

Direct measurements of LyC emission can be used for estimating the average $f_{\rm esc}$(LyC) at $z \sim 3$, and the relationships between $f_{\rm esc}$(LyC) and other galaxy properties. Determining these relationships is crucial for translating measurements of non-ionizing radiation from galaxies during the epoch of reionization into an estimate of their contribution to the ionizing budget.

Robust detections of LyC emission have recently been obtained for several low-redshift galaxies using COS on the *Hubble Space Telescope* (*HST*) (e.g., Borthakur et al. 2014; Izotov et al. 2016; Leitherer et al. 2016). At $z \sim 3$, both spectroscopic (e.g., Shapley et al. 2006) and ground-based and *HST* imaging techniques have been used to measure LyC emission (e.g., Nestor et al. 2011; Mostardi et al. 2013; Grazian et al. 2016; Vanzella et al. 2012). In ground-based $z \sim 3$ LyC observations, contamination by lower-redshift interlopers is a serious concern. When contaminated, the flux at $\sim 3500$Å observed does not consist of LyC at $z \sim 3$, but rather non-ionizing UV-continuum from a lower-redshift source near the line of sight. High-spatial-resolution observations (e.g., with *HST*) are required to rule out contamination (Vanzella et al. 2012). To date, there is only one object with a spectroscopic detection of LyC at $z \sim 3$ and uncontaminated *HST* morphology, i.e., *Ion2* at $z = 3.21$ (de Barros et al. 2016; Vanzella et al. 2016).

As we describe here, we have obtained deep Keck/LRIS spectroscopy for a large sample of Lyman Break Galaxies (LBGs) at $z \sim 3$, including coverage of the LyC region (Steidel et al., in prep.). Roughly 10% of these galaxies show spectroscopic detections of LyC radiation. One of them, Q1549-C25, is also covered by multi-wavelength *HST* imaging, from which we determine that the galaxy is unaffected by low-redshift contamination and represents a clean detection of LyC emission. In §2, we describe our spectroscopic and imaging observations. In §3, we present the spectroscopic detection

Electronic address: aes@astro.ucla.edu

[1] Based on data obtained at the W.M. Keck Observatory, which is operated as a scientific partnership among the California Institute of Technology, the University of California, and the National Aeronautics and Space Administration, and was made possible by the generous financial support of the W.M. Keck Foundation.

[2] Department of Physics and Astronomy, University of California, Los Angeles, 430 Portola Plaza, Los Angeles, CA 90095, USA
[3] Cahill Center for Astronomy and Astrophysics, California Institute of Technology, 1216 East California Boulevard., MS 249-17, Pasadena, CA 91125, USA
[4] Astronomical Observatory, Volgina 7, 11060 Belgrade, Serbia
[5] Department of Physics and Astronomy, University of California, Riverside, 900 University Avenue, Riverside, CA 92521, USA
[6] Physics Department, Los Positas College, 3000 Campus Hill Drive Livermore CA 94551, USA
[7] Carnegie Observatories, 813 Santa Barbara Street, Pasadena, CA 91101, USA

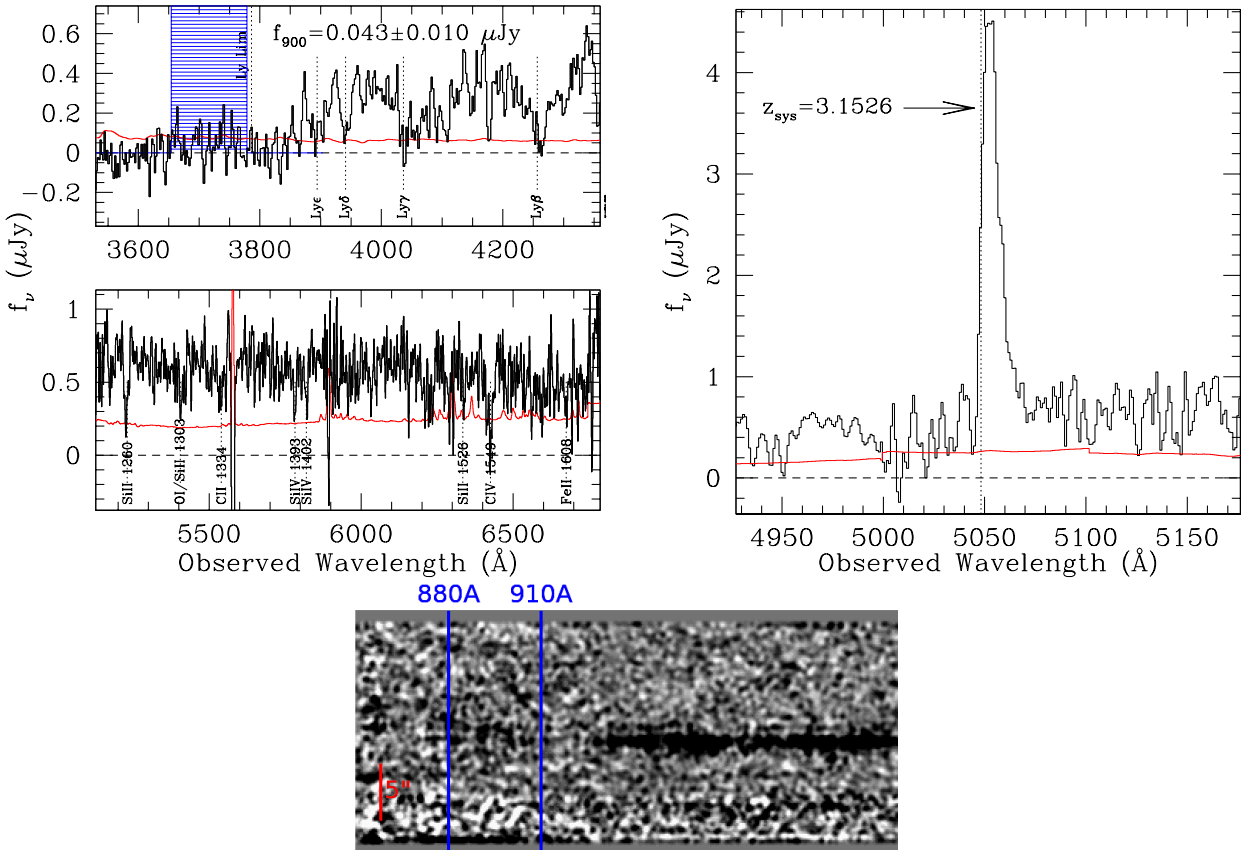


**Figure 1.** **Top:** Deep LRIS spectrum of Q1549-C25. The spectrum is presented in the observed frame, and the flux-density units are $\mu$Jy. The error spectrum is plotted in red. Blue- and red-side spectra are joined together at the 5000 Å dichroic cut-off. **Top left:** The top panel shows the LyC range ($880-910$Å), indicated as a blue shaded region, and Lyman-series absorption lines. $f_{900}$ is evaluated as the mean flux-density in the LyC region. The bottom panel shows the spectral range longwards of Ly$\alpha$, containing several labeled interstellar metal absorption lines. **Top right:** Zoomed-in spectrum of Ly$\alpha$ emission. The Ly$\alpha$ profile profile is characterized by a single emission peak offset relative to the systemic redshift of Q1549-C25, indicated by the vertical dotted line. **Bottom:** Two-dimensional spectrum of Q1549-C25, with the LyC region bracketed by vertical blue lines at rest wavelengths of 880 and 990Å. Wavelength increases from left to right and the spatial scale is indicated with a vertical bar of 5" in extent. The spectrum has been lightly smoothed by a Gaussian kernel with 3-pixel radius.

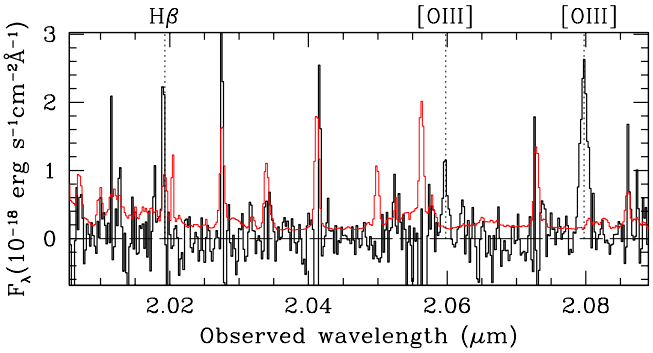


**Figure 2.** MOSFIRE $K$-band spectrum of Q1549-C25. The spectrum is presented in the observed frame and the flux-density units are $10^{-18}$ ergs s$^{-1}$ cm$^{-2}$ Å$^{-1}$. The error spectrum is plotted in red. The [OIII]$\lambda$5007 and [OIII]$\lambda$4959 lines are clearly detected, while H$\beta$ falls on a sky line. The combined [OIII]+H$\beta$ emission-line flux is $\leq 5.2\times10^{-17}$ergs s$^{-1}$ cm$^{-2}$, corresponding to a rest-frame equivalent width of $W_{([\mathrm{OIII}]+\mathrm{H}\beta),0}\leq 256$Å. The systemic redshift based on [OIII] emission is $z_{sys}=3.1526$.

of LyC emission in Q1549-C25, along with the galaxy's multi-wavelength morphology and stellar population parameters. Finally, in §4, we discuss the implications for estimating $f_{\rm esc}$(LyC), compare the properties of $z\sim3$ galaxies detected in LyC, and consider the outlook for LyC observations at high redshift. Throughout, we adopt cosmological parameters of $H_0 = 70$ km s$^{-1}$ Mpc$^{-1}$, $\Omega_M = 0.30$, and $\Omega_\Lambda = 0.7$.

## 2. OBSERVATIONS & METHODS

### 2.1. *Keck Spectroscopy*

As described in Steidel et al. (in prep.), we used the LRIS spectrograph on the Keck I telescope to assemble a sample of 136 galaxies at $2.72\leq z\leq 3.52$ ($\langle z\rangle = 3.05\pm0.18$) with deep rest-UV spectra covering the LyC region (rest-frame $880-910$Å). The galaxy Q1549-C25 has coordinates of R.A.=15:52:06.07 and decl.=+19:11:28.4 (J2000), $\mathcal{R}_{AB} = 24.83$ (i.e., roughly $L^*$; Reddy et al. 2008), and falls in the HS1549+1919 field, one of the survey fields of the Keck Baryonic Structure Survey (KBSS; Rudie et al. 2012; Steidel et al. 2014). This object was originally identified as a $z\sim3$ photometric candidate and confirmed at $z_{Ly\alpha}=3.16$ using, respectively, LRIS $U_nG\mathcal{R}$ imaging and spectroscopy (Steidel et al. 2003; Reddy et al. 2008). In subsequent deep LyC

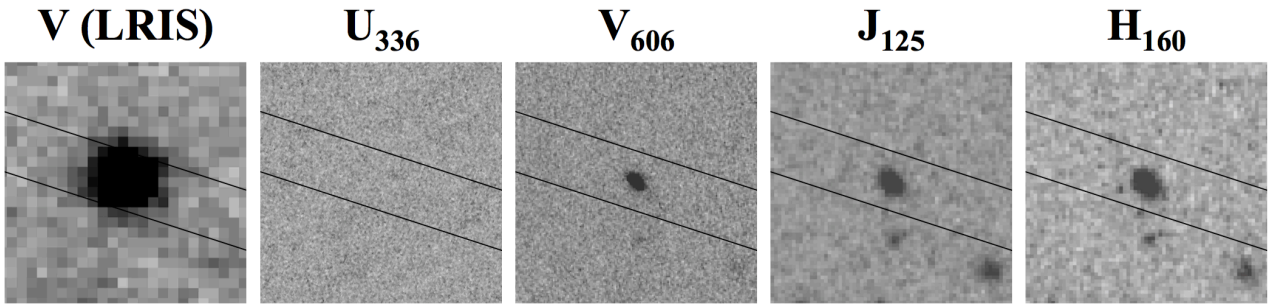


**Figure 3.** 5" × 5" postage stamp images of Q1549-C25. From left to right, we show ground-based $V$ band, $U_{336}$, $V_{606}$, $J_{125}$, and $H_{160}$, oriented with north up and east to the left. The LRIS slit is overlaid on each postage stamp. These images indicate that C25 consists of a single component within a 1" radius. The faint galaxy 1.″3 to the south does not contribute to the flux measured in the LRIS spectrum. The lack of $U_{336}$ detection for Q1549-C25 is consistent with the spectroscopic detection of $f_{900}$, given the depth of the $U_{336}$ imaging.

spectroscopy, Q1549-C25 was observed through a multi-object slitmask with 1.″2 slits, at a sky position angle of $\theta = 72°$. Data were collected in April and June 2008, for a total exposure time of 8.4 hours under photometric conditions and seeing ∼0.″5−0.″7. LRIS was configured with the "d500" dichroic, sending wavelengths shorter and longer than 5000Å, respectively, to the blue and red channels, where they were dispersed, respectively, by a 400 lines/mm grism blazed at 3400Å, and 600 lines/mm grating blazed at 5000Å.

LRIS spectroscopic data were reduced as described in Steidel et al. (in prep.). In brief, individual two-dimensional spectra were flatfielded, cut out, rectified, corrected for non-uniform slit illumination, background-subtracted, combined, extracted to one dimension, and wavelength and flux-calibrated. The spectra were also dereddened for Galactic extinction, using $E(B-V) = 0.045$ for the HS1549+1919 field (Schlegel et al. 1998). When trying to detect the faint signal of LyC emission, it is crucial to minimize and quantify the systematic and statistical uncertainties associated with these steps. We used careful tests for residual systematic errors in background subtraction to establish that the zero flux level was robustly estimated (see Steidel et al., in prep for details),[8] a significant improvement over previous analyses (e.g., Shapley et al. 2006).

A Keck/MOSFIRE $K$-band spectrum was obtained for Q1549-C25 in May 2016, for a total of 1.5 hours in photometric conditions with 0.″7 seeing. Observations were performed and data reduced as described in Steidel et al. (2014).

### 2.2. *HST and Other Imaging*

We have obtained deep *HST* imaging in two pointings in the HS1549+1919 field (Mostardi et al. 2015). Each pointing is covered by WFC3/UVIS $U_{336}$ (5 orbits), ACS/WFC $V_{606}$ (5 orbits), WFC3/IR $J_{125}$ (3 orbits) and $H_{160}$ (3 orbits). These pointings were chosen to optimize the number of LBGs and Ly$\alpha$ emitters (LAEs) with apparent LyC emission detections inferred from 3420Å narrow-band imaging (Mostardi et al. 2013). Despite not being detected at 3420Å, Q1549-C25 has coverage in all four *HST* bands, enabling a careful analysis of its multi-wavelength morphology.

In addition, there is ground-based optical and near-IR imaging, as well as *Spitzer*/IRAC photometry for Q1549-C25. These include the original Keck/LRIS $U_nG\mathcal{R}$ plus $V$-band imaging, $J$ and $K_s$ from Palomar/WIRC (Reddy et al. 2012), $K_s$ and medium-band $J_1$, $J_2$, $J_3$, $H_{short}$, and $H_{long}$ from Magellan/FourStar, and IRAC channels 2 ($4.5\mu m$) and 4 ($8.0\mu m$). Q1549-C25 is detected in all bands except $U_{336}$, $U_n$, $J$, $H_{long}$, and IRAC channel 4.

## 3. RESULTS

### 3.1. *The Direct Detection of LyC*

Q1549-C25 is one of 13 galaxies in the LRIS LyC sample with a $\geq 3\sigma$ detection of $f_{900}$, the average flux density at rest-frame $880-910$Å. The rest-frame UV spectrum of Q1549-C25 is shown in Figure 1. The top left panel highlights the LyC region, in which we measure $f_{900} = 0.043\pm0.010$ $\mu$Jy, corresponding to an AB magnitude of $m_{900} = 27.33\pm0.26$. The bottom panel shows the two-dimensional spectrum of Q1549-C25 over the LyC region, where a faint signal is apparent. The average non-ionizing UV flux density is estimated from the LRIS spectrum over the rest-frame range $1480-1520$Å, yielding $f_{1500} = 0.523\pm0.019$ $\mu$Jy. Combining these measurements, we find $f_{900}/f_{1500} = 0.08 \pm 0.02$ for the ratio of ionizing to non-ionizing flux density.

The rest-frame UV spectrum of Q1549-C25 features strong Ly$\alpha$ emission (rest-frame equivalent width, $W_{Ly\alpha,0} = 15$ Å) at $z_{Ly\alpha} = 3.156$ (see Figure 1, top right) and several low- (Si II $\lambda$1260, OI+Si II $\lambda$1303, C II $\lambda$1334, Si II $\lambda$1526, Fe II $\lambda$1608) and high-ionization (Si IV $\lambda\lambda1393, 1402$, C IV $\lambda\lambda1548, 1550$) interstellar metal absorption features at $z_{abs} = 3.149$ (top left panel). The difference between Ly$\alpha$ emission and interstellar absorption redshifts arises due to large-scale outflow motions in the ISM of Q1549-C25 (e.g., Pettini et al. 2001; Shapley et al. 2003). The systemic redshift, $z_{sys} = 3.1526$, is measured from the [OIII]$\lambda$5007 emission centroid in the MOSFIRE spectrum (Figure 2).

Multiple Lyman-series absorption lines are also detected in the spectrum of Q1549-C25, although their pro-

[8] As described in Steidel et al. (in prep.), we performed multiple careful tests of our background subtraction. In one such test, we created a stack of 10 two-dimensional spectra with LyC detections (including the spectrum of Q1549-C25), registering the individual spectra at the position of each target galaxy. From this two-dimensional stack, we extracted spectra over the wavelength regions $3450-3650$Å and $4000-4100$Å, including all pixels along the slit except those within ±4" of the stacked target position. The resulting pixel flux distributions in each of these wavelength regions are centered on zero counts, in agreement with pure Gaussian noise, with a standard deviation as expected by our noise model including photon counting statistics and detector read noise.

files may be contaminated by absorption from intervening Ly$\alpha$ forest features. Given the high signal-to-noise of the spectrum, it is finally worth noting that there is no evidence of a spectroscopic "blend" with a lower-redshift object along the line of sight. Such contamination would have appeared in the form of absorption or emission features corresponding to an additional, lower redshift (see, e.g., Figure 5 of Siana et al. 2015).

### 3.2. *Multi-wavelength Morphology*

Q1549-C25 is the only galaxy in our LRIS LyC sample with a significant LyC detection for which multi-wavelength *HST* imaging also exists. Figure 3 shows ground-based $V$-band, along with *HST* $U_{336}V_{606}J_{125}H_{160}$ imaging. In contrast to the majority of $z \sim 3$ apparent sources of LyC emission (Vanzella et al. 2012; Mostardi et al. 2015; Siana et al. 2015), Q1549-C25 consists of a single source of emission at *HST* resolution, with no nearby sources of potential contamination to the LRIS spectrum. The closest source to Q1549-25 is at a radial separation of 1.″3 in the southern direction, well outside the LRIS slit, significantly fainter than Q1549-C25 at all wavelengths, and undetected in $U_{336}$. Although there are two apparent positive fluctuations at separations of 0.″5–0.″6 from Q1549-C25 in the $H_{160}$ image (one of which also corresponds to a positive fluctuation in the $J_{125}$ image), these are not significant and have no counterparts in $U_{336}$ or $V_{606}$. Mostardi et al. (2015) performed a detailed analysis of the multi-wavelength morphologies and photometry of 16 LBGs in the HS1549+1919 field covered by $U_{336}V_{606}J_{125}H_{160}$ imaging, using the $V_{606}$ image for detecting objects and defining isophotes with *SExtractor* (Bertin & Arnouts 1996). In this analysis, Q1549-C25 was described by a single segment, with uniform morphology in $V_{606}$, $J_{125}$, and $H_{160}$, and classified as "uncontaminated."

The $U_{336}$ filter provides a clean probe of the LyC spectral region at $z = 3.15$, and therefore a potential window on the morphology of escaping LyC emission. However, as shown in Figure 3, Q1549-C25 is undetected in $U_{336}$. This non-detection is entirely consistent with the spectroscopic detection of LyC emission, given the depth of the $U_{336}$ image. Using an isophote defined by $V_{606}$, we measure a $3\sigma$ upper limit of $m_{336} = 26.80$, consistent with the LRIS LyC detection, based on the assumption of a flat spectrum between rest-frame $880 - 910$Å and the effective rest wavelength of the F336W filter, i.e., 808Å (which is the most optimistic case, given the likely increased IGM attenuation at shorter wavelengths).

### 3.3. *Stellar Population Modeling*

We used the Bruzual & Charlot (2003) population synthesis code to model the spectral energy distribution (SED) of Q1549-C25, characterizing its stellar population and dust content. For such modeling, we fit ground-based $G$, $\mathcal{R}$, $J_1$, $J_2$, $J_3$, $H_{short}$, along with *HST* $V_{606}$, $J_{125}$, and $H_{160}$ and *Spitzer*/IRAC channel 2, correcting $G$ and $V_{606}$ beforehand for the contribution from Ly$\alpha$ emission ($W_{Ly\alpha,0} = 15$Å), and $K_s$ for the combined contribution of [OIII] and H$\beta$ ($W_{([\mathrm{OIII}]+\mathrm{H}\beta),0} = 256$Å). Based on a constant star formation (CSF), solar-metallicity model, Chabrier IMF, and Calzetti et al. (2000) extinction curve, we find $E(B-V) = 0.0^{+0.0}_{-0.0}$, Age$= 1.3^{+0.5}_{-0.4}$ Gyr, SFR$=6^{+0}_{-1}$ $M_\odot$ yr$^{-1}$, and $M_* = 7.9^{+2.5}_{-2.3} \times 10^9 M_\odot$, where parameter confidence intervals reflect the photometric uncertainties.[9] Assuming an exponentially-rising star-formation history yields very similar best-fit parameters. Figure 4 shows the SED of Q1549-C25, along with the best-fit CSF model.

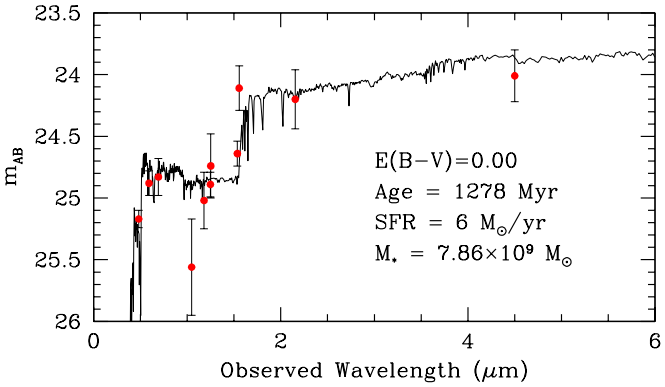


**Figure 4.** Observed and best-fit model SEDs for Q1549-C25. $G$ and $V_{606}$ have been corrected for Ly$\alpha$ emission, while $K_s$ has been corrected for emission from [OIII]$\lambda$5007 and H$\beta$. The parameters for the best-fit CSF model are indicated in the legend.

## 4. DISCUSSION

### 4.1. *The LyC Escape Fraction*

We can estimate the LyC escape fraction of Q1549-C25 based on the observed LyC to non-ionizing UV flux-density ratio, $f_{900}/f_{1500}$, the intrinsic luminosity-density ratio, $L_{900}/L_{1500}$, and the IGM transmission factor, $t_{IGM}$. The escape fraction is typically quoted in both *relative* and *absolute* terms. The relative escape fraction, $f_{\mathrm{esc,rel}}(\mathrm{LyC})$ is a measure of how the observed $f_{900}/f_{1500}$ ratio (corrected for IGM absorption) compares to the theoretical one, while the absolute escape fraction, $f_{\mathrm{esc}}(\mathrm{LyC})$, is simply the ratio of the escaping to intrinsic LyC luminosity density. In terms of the quantities described above, we define $f_{\mathrm{esc,rel}}(\mathrm{LyC})$ as:

$$f_{\mathrm{esc,rel}}(\mathrm{LyC}) = \frac{(f_{900}/f_{1500})}{(L_{900}/L_{1500})t_{IGM}} \quad (1)$$

The absolute escape fraction is defined as:

$$f_{\mathrm{esc}}(\mathrm{LyC}) = f_{\mathrm{esc,rel}}(\mathrm{LyC}) \times f_{\mathrm{esc}}(1500) \quad (2)$$

where $f_{\mathrm{esc}}(1500)$ refers to the absolute escape fraction at 1500Å, modulated by dust attenuation. Since $E(B-V) = 0$ for Q1549-C25, $f_{\mathrm{esc}}(1500) = 1$, and $f_{\mathrm{esc}}(\mathrm{LyC}) = f_{\mathrm{esc,rel}}(\mathrm{LyC})$. Therefore, equation 1 can be rewritten as:

$$f_{900}/f_{1500} = f_{\mathrm{esc}}(\mathrm{LyC})(L_{900}/L_{1500})t_{IGM} \quad (3)$$

Our measurement of $f_{900}/f_{1500} = 0.08 \pm 0.02$ constrains the quantity, $f_{\mathrm{esc}}(\mathrm{LyC})(L_{900}/L_{1500})t_{IGM}$. A precise estimate of $f_{\mathrm{esc}}(\mathrm{LyC})$ is not possible, given the uncertainties in $t_{IGM}$ for a single $z = 3.15$ sightline (Vanzella et al. 2016), and, to a lesser extent, $L_{900}/L_{1500}$. However, based on reasonable assumptions, we can place rough constraints on $f_{\mathrm{esc}}(\mathrm{LyC})$.

[9] 91% of Monte Carlo realizations of the best-fit model yielded $E(B-V) = 0$.

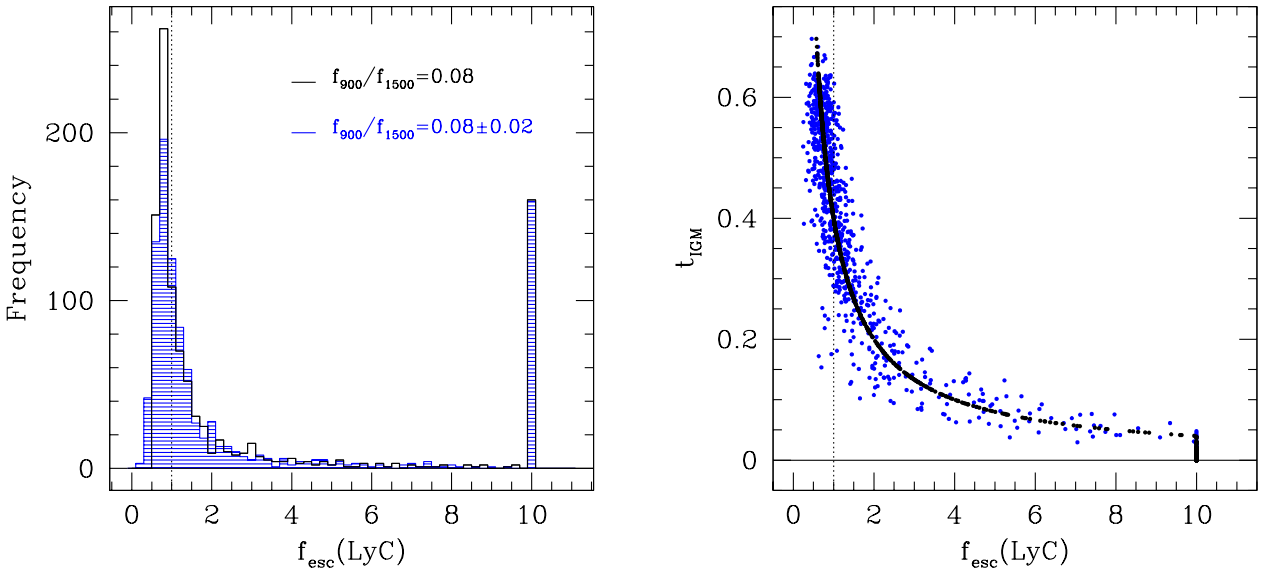


**Figure 5.** Distribution of $f_{\rm esc}$(LyC) for Q1549-C25. $f_{\rm esc}$(LyC) is estimated based on the observed $f_{900}/f_{1500}$, an assumed intrinsic ratio, $L_{900}/L_{1500} = 0.20$, and 1000 simulated realizations of IGM+CGM transmission in the LyC region at $z = 3.15$. In each panel, black symbols result from assuming no measurement uncertainty in $f_{900}/f_{1500}$, while blue ones assume the observed error of 0.02. Values of $f_{\rm esc}$(LyC) $> 10$ (i.e., resulting from low $t_{IGM}$) have been fixed at 10, and $f_{\rm esc}$(LyC) $= 1$ is indicated as a vertical dotted line. **Left:** Histogram of $f_{\rm esc}$(LyC) for Q1549-C25. $f_{\rm esc}$(LyC) $\leq 1$ corresponds to 45% of the realizations. **Right:** Joint distribution of $t_{IGM}$ vs. $f_{\rm esc}$(LyC). With the assumption of no error bar in $f_{900}/f_{1500}$, there is a one-to-one relation between $t_{IGM}$ and $f_{\rm esc}$(LyC).

In order to investigate constraints on $f_{\rm esc}$(LyC), we generated 1000 model $z = 3.15$ sightlines simulating the distribution of H I absorbers in both the IGM and circumgalactic medium (CGM), the latter reflecting the the enhancement in intergalactic H I absorption in the vicinity of high-redshift star-forming galaxies. The absorber distributions were based on observations from Rudie et al. (2012) and Rudie et al. (2013), and are described in more detail in Steidel et al. (in prep). For each model sightline, we calculated the average transmission factor, $t_{IGM}$, over the rest wavelength range, $880 - 910$Å. We also considered the intrinsic luminosity-density ratio, $L_{900}/L_{1500}$, with $L_{900}$ and $L_{1500}$ defined in units of ergs s$^{-1}$Hz$^{-1}$. For an age of $\sim 1$ Gyr, solar-metallicity CSF models predict $L_{900}/L_{1500}$ ranging from $0.14 - 0.25$ (Bruzual & Charlot 2003; Siana et al. 2007; Stanway et al. 2016). Larger values are possible for lower metallicities or different assumptions regarding massive stellar evolution. We adopted $L_{900}/L_{1500} = 0.20$ as a fiducial value.

Based on the ensemble of simulated $z = 3.15$ sightlines, the measurement and uncertainty in $f_{900}/f_{1500}$, and the assumed value of $L_{900}/L_{1500} = 0.20$, we calculated the distribution of $f_{\rm esc}$(LyC) (Figure 5, left, blue shaded histogram). We find that slightly less than half (45%) of the distribution of $f_{\rm esc}$(LyC) is at $\leq 1$, and 95% of the distribution is at $f_{\rm esc}$(LyC) $\geq 0.51$. The results are very similar if, instead of assuming $L_{900}/L_{1500} = 0.20$, we randomly draw $L_{900}/L_{1500}$ values uniformly between 0.14 and 0.25. It is also useful to visualize the inverse relationship between $t_{IGM}$ and $f_{\rm esc}$(LyC), given $f_{900}/f_{1500}$ and $L_{900}/L_{1500}$ (Figure 5, right). With no measurement error (black points), a requirement of $f_{\rm esc}$(LyC) $\leq 1$ translates into an IGM transmission factor of $t_{IGM} \geq 0.40$, which is higher than the average at $z = 3.15$. Scatter is introduced into the $t_{IGM}$ vs. $f_{\rm esc}$(LyC) relationship by the measurement uncertainty in $f_{900}/f_{1500}$ (blue points), yet the requirement of $f_{\rm esc}$(LyC) $\leq 1$ implies a mean transmission of $\langle t_{IGM} \rangle = 0.519$, which is significantly higher than through a random $z = 3.15$ sightline ($\langle t_{IGM}(z = 3.15) \rangle = 0.339$).

### 4.2. *A Comparison of Q1549-C25 and Ion2*

The only other $z \sim 3$ galaxy with a direct spectroscopic detection of uncontaminated LyC emission is *Ion2* at $z = 3.21$ (de Barros et al. 2016; Vanzella et al. 2016). It is therefore useful to compare the properties of *Ion2* and Q1549-C25. In terms of the escape of LyC emission, *Ion2* appears more extreme than Q1549-C25. de Barros et al. (2016) report $f_{900}/f_{1500} = 0.11$ (S/N $\sim 5$) for *Ion2*. Using the same IGM+CGM model tuned to $z = 3.2$, and the same assumed value for $L_{900}/L_{1500}$, we find that 95% of the distribution of $f_{\rm esc}$(LyC) is at $\geq 0.79$ for *Ion2*. *Ion2*, like Q1549-C25, is characterized by negligible dust extinction, and therefore $f_{\rm esc,rel}$(LyC) $= f_{\rm esc}$(LyC). de Barros et al. (2016) report a significantly lower escape fraction for *Ion2* ($f_{\rm esc}$(LyC) $= 0.64 \pm 0.1$), but assume a more transparent model for IGM opacity (Inoue et al. 2014), and $L_{900}/L_{1500} = 1/3$. Regardless of the particular IGM model assumed, both sources are characterized by significantly higher $f_{900}/f_{1500}$ values and $f_{\rm esc}$(LyC) distributions than average at $z \sim 3$ (Steidel et al., in prep), suggesting large variations in these quantities among high-redshift star-forming galaxies.

Along with a higher $f_{900}/f_{1500}$, *Ion2* also has significantly larger rest-frame Ly$\alpha$ and [OIII]$\lambda$5007 emission equivalent widths than Q1549-C25, with $W_{Ly\alpha,0} = 94$ Å and $W_{\rm [OIII],0} = 1500$ Å. In addition, no low-ionization metal absorption lines are detected in the rest-UV spectrum of *Ion2*, suggesting a lower covering fraction of neutral gas than the spectrum of Q1549-C25, in which sev-

eral low-ionization lines are detected. Finally, the Ly$\alpha$ profile of *Ion2* is double-peaked, with the centroid of the blue peak coinciding with the galaxy systemic redshift. Comparing this profile with Ly$\alpha$ radiative transfer models, de Barros et al. (2016) cite it as evidence for a low neutral gas column density. The Ly$\alpha$ profile of Q1549-C25 on the other hand is described by a single peak (at a resolution of $R \sim 1400$, higher than that of the VLT/VIMOS spectrum of *Ion2*), which is redshifted by 500 km s$^{-1}$ relative to the interstellar absorption lines, and 250 km s$^{-1}$ with respect to the systemic redshift. The large-scale outflow in Q1549-C25, reflected by the offsets of Ly$\alpha$ and interstellar absorption redshifts (Shapley et al. 2003) relative to systemic, may yield a porous ISM whose gaps provide escape routes for LyC photons.

As stated above, the stellar population fits for both galaxies imply $E(B-V) \sim 0$, which is conducive to the escape of LyC radiation, and SFRs and stellar masses lower than the median for $\mathcal{R} \leq 25.5$ LBGs (SFR $= 6M_\odot$ yr$^{-1}$ and $M_* = 7.9 \times 10^9 M_\odot$ for Q1549-C25, and SFR $= 16M_\odot$ yr$^{-1}$ and $M_* = 3.2 \times 10^9 M_\odot$ for *Ion2*). The best-fit age for Q1549-C25 is $\sim 1$ Gyr, while it is 400 Myr for *Ion2*. Both of these are older than the median CSF age derived for LBGs (Kornei et al. 2010), which is notable, given that the intrinsic ratio of LyC to non-ionizing UV luminosity density, $L_{900}/L_{1500}$, is highest at young ages ($\leq 10$ Myr) and declines to a minimum value at ages $> 300$ Myr (assuming continuous star formation; Siana et al. 2007). Mostardi et al. (2015) present photometric evidence that the galaxy, Q1549-MD5b is leaking LyC radiation, and described by an age of only 50 Myr. Accordingly, LyC leakage appears to occur over a wide range in galaxy age.

### 4.3. *Outlook*

The direct and uncontaminated spectroscopic detection of LyC emission has now been achieved for two galaxies at $z \sim 3$. Based on reasonable assumptions, both sources suggest high escape fractions ($\gtrsim 0.5$), though the constraints on $f_{\rm esc}$(LyC) are not precise. Both sources are characterized by negligible dust extinction and strong Ly$\alpha$ emission, and, contrary to simple expectations, stellar population ages older than the median for $z \sim 3$ LBGs. In order to make progress on estimating the typical LyC escape fraction at $z \sim 3$ and during the epoch of reionization, we now require an order-of-magnitude larger sample of galaxies with clean detections of LyC emission. With such a sample, averaged over many sightlines, the constraints on the mean IGM transmission and therefore $f_{\rm esc}$(LyC) will be much stronger. Our survey of LBGs with deep LRIS spectroscopy of the LyC region has yielded 13 galaxies, including Q1549-C25, with apparent spectroscopic detections of LyC and no evidence of blending from lower-redshift interlopers. Observations at the spatial resolution of *HST* will enable us to rule out possible contamination and characterize the global contribution of star-forming galaxies at $z \geq 3$ to the ionizing background.

## ACKNOWLEDGEMENTS

We thank the anonymous referee for a constructive report. CCS acknowledges support from NSF grants AST-0908805 and AST-1313472. AES acknowledges support from the David & Lucile Packard Foundation. NAR is supported by an Alfred P. Sloan Research Fellowship. We wish to extend special thanks to those of Hawaiian ancestry on whose sacred mountain we are privileged to be guests. Without their generous hospitality, most of the observations presented herein would not have been possible.

## REFERENCES

Bertin, E., & Arnouts, S. 1996, A&AS, 117, 393
Borthakur, S., Heckman, T. M., Leitherer, C., & Overzier, R. A. 2014, Science, 346, 216
Bruzual, G., & Charlot, S. 2003, MNRAS, 344, 1000
Calzetti, D., Armus, L., Bohlin, R. C., et al. 2000, ApJ, 533, 682
de Barros, S., Vanzella, E., Amorín, R., et al. 2016, A&A, 585, A51
Finkelstein, S. L., Papovich, C., Ryan, R. E., et al. 2012, ApJ, 758, 93
Grazian, A., Giallongo, E., Gerbasi, R., et al. 2016, A&A, 585, A48
Inoue, A. K., Shimizu, I., Iwata, I., & Tanaka, M. 2014, MNRAS, 442, 1805
Izotov, Y. I., Orlitová, I., Schaerer, D., et al. 2016, Nature, 529, 178
Kornei, K. A., Shapley, A. E., Erb, D. K., et al. 2010, ApJ, 711, 693
Kuhlen, M., & Faucher-Giguère, C.-A. 2012, MNRAS, 423, 862
Leitherer, C., Hernandez, S., Lee, J. C., & Oey, M. S. 2016, ArXiv e-prints, arXiv:1603.06779
Mostardi, R. E., Shapley, A. E., Nestor, D. B., et al. 2013, ApJ, 779, 65
Mostardi, R. E., Shapley, A. E., Steidel, C. C., et al. 2015, ApJ, 810, 107
Nestor, D. B., Shapley, A. E., Steidel, C. C., & Siana, B. 2011, ApJ, 736, 18
Pettini, M., Shapley, A. E., Steidel, C. C., et al. 2001, ApJ, 554, 981
Reddy, N. A., Pettini, M., Steidel, C. C., et al. 2012, ApJ, 754, 25
Reddy, N. A., Steidel, C. C., Pettini, M., et al. 2008, ApJS, 175, 48
Robertson, B. E., Ellis, R. S., Furlanetto, S. R., & Dunlop, J. S. 2015, ApJ, 802, L19
Rudie, G. C., Steidel, C. C., Shapley, A. E., & Pettini, M. 2013, ApJ, 769, 146
Rudie, G. C., Steidel, C. C., Trainor, R. F., et al. 2012, ApJ, 750, 67
Schlegel, D. J., Finkbeiner, D. P., & Davis, M. 1998, ApJ, 500, 525
Shapley, A. E., Steidel, C. C., Pettini, M., & Adelberger, K. L. 2003, ApJ, 588, 65
Shapley, A. E., Steidel, C. C., Pettini, M., Adelberger, K. L., & Erb, D. K. 2006, ApJ, 651, 688
Siana, B., Teplitz, H. I., Colbert, J., et al. 2007, ApJ, 668, 62
Siana, B., Shapley, A. E., Kulas, K. R., et al. 2015, ApJ, 804, 17
Stanway, E. R., Eldridge, J. J., & Becker, G. D. 2016, MNRAS, 456, 485
Steidel, C. C., Adelberger, K. L., Shapley, A. E., et al. 2003, ApJ, 592, 728
Steidel, C. C., Rudie, G. C., Strom, A. L., et al. 2014, ApJ, 795, 165
Vanzella, E., Guo, Y., Giavalisco, M., et al. 2012, ApJ, 751, 70
Vanzella, E., de Barros, S., Vasei, K., et al. 2016, ArXiv e-prints, arXiv:1602.00688